J Nanostruct 16(3): 3869-3883, Summer 2026

RESEARCH PAPER

# Highly Removal of Crystal Violet Dye Using $SnO_2/Fe_2O_3$@RGO Nanocomposite in Batch Adsorption Systems: Isotherm, Kinetic, Thermodynamic, and Regeneration Studies

*Hiba J. Turki [1]*, Faiq F. Karam [2], Hajar Fadhil Abed Alzahra [1], Khamael Abdulsalam Abed [3]*

[1] *Department of Forensic Science, College of Science, University of Al-Qadisiyah, Diwaniyah, Iraq*
[2] *Department of Chemistry, College of Science, University of Al-Qadisiyah, Diwaniyah, Iraq*
[3] *Department of Environment, College of Science, University of Al-Qadisiyah, Diwaniyah, Iraq*

## ARTICLE INFO

***Article History:***
*Received 06 April 2026*
*Accepted 20 June 2026*
*Published 01 July 2026*

***Keywords:***
*Adsorption*
*Crystal Violet Dye*
*Nanocomposite*
*Reduced graphene oxide*
*Water purification*

## ABSTRACT

A ternary composite of tin oxide ($SnO_2$), iron oxide ($Fe_2O_3$), and reduced graphene oxide (RGO) was synthesized and applied as an efficient adsorbent for removing Crystal Violet (CV) dye from aqueous solutions. The effects of various parameters including adsorbent dosage, contact time, temperature, pH, and ionic strength were systematically studied. pH was identified as the most significant factor, with optimal removal (93.5%) achieved at pH 9. The maximum adsorption capacity reached 51.2 mg/g at 298 K. Kinetic analysis revealed that the adsorption followed the pseudo-second-order model ($R^2$ = 0.9969), while the Freundlich isotherm model best described the equilibrium data ($R^2$ = 0.9653). Thermodynamic parameters ($\Delta G°$, $\Delta H°$, $\Delta S°$) indicated a spontaneous and exothermic process, suggesting physical adsorption. Regeneration tests showed a decline in efficiency from 94.9% to 60.6% over five cycles, confirming acceptable reusability. The material structure was characterized to validate composite formation. Compared to individual components, the composite showed superior performance. These results confirm the promising potential of $SnO_2/Fe_2O_3$@RGO as a cost-effective, reusable, and environmentally friendly adsorbent for treating dye-contaminated water in wastewater treatment applications.

**How to cite this article**
*Turki H, Karam F, Abed Alzahra H, Abed KH. Highly Removal of Crystal Violet Dye Using $SnO_2/Fe_2O_3$@RGO Nanocomposite in Batch Adsorption Systems: Isotherm, Kinetic, Thermodynamic, and Regeneration Studies. J Nanostruct, 2026; 16(3):3869-3883. DOI: 10.22052/JNS.2026.03.073*

## INTRODUCTION

Water is a vital resource, comprising nearly 60 % of the human body and essential for agriculture, industry, and public health [1–2]. However, untreated industrial wastewater especially from textile and dyeing sectors has increasingly polluted global water bodies [3–4]. Synthetic dyes such as Crystal Violet (CV) are persistent pollutants with complex aromatic structures that resist biodegradation [5–6]. Approximately 15 % of the dyes used industrially are discharged untreated into waterways, posing severe risks to

* *Corresponding Author Email: hiba.jaleel@qu.edu.iq*

aquatic ecosystems and human health [7–8]. CV, a cationic triphenylmethane dye widely used in textile, printing, and biomedical applications, is recognized for its high toxicity, carcinogenicity, and mutagenicity at even low concentrations [9–10]. Therefore, efficient removal of CV from wastewater is imperative to mitigate environmental and health hazards. Various treatment technologies—such as membrane filtration, coagulation-flocculation, advanced oxidation, and biological degradation—have been explored for dye removal [11–12]. Among these, adsorption stands out due to its simplicity, high removal efficiency, cost-effectiveness, and regenerability, particularly when low-cost adsorbents are used [13–14]. Advancements in nanotechnology have introduced novel composite adsorbents combining metal oxides with carbon-based materials to enhance adsorption performance [15]. Reduced graphene oxide (RGO) offers a large surface area and excellent conductivity, while metal oxides like $SnO_2$ and $Fe_2O_3$ provide active adsorption and catalytic sites [16]. The ternary composite $SnO_2/Fe_2O_3$@RGO exhibits synergistic effects—enhancing adsorption capacity and regeneration potential compared to individual components [17]. Although earlier studies have applied $SnO_2/Fe_2O_3$@RGO mainly in photocatalytic dye degradation, its use in adsorption—especially for CV removal—has been seldom examined [18]. Moreover, literature on CV adsorption using RGO-metal oxide systems often lacks comprehensive kinetic, isothermal, thermodynamic, and reusability data [19–20].

This study aims to synthesize and thoroughly characterize $SnO_2/Fe_2O_3$@RGO as a novel, efficient adsorbent for CV removal from aqueous solutions. It evaluates the impacts of operational parameters (adsorbent dosage, contact time, pH, temperature, and ionic strength), and performs adsorption kinetics, isotherm, thermodynamic, and regeneration analyses to determine both mechanism and field applicability.

## MATERIALS AND METHODS

### *Materials and Instrumentals*

The laboratory apparatus used in this study included analytical balances, magnetic stirrers, hotplates, burettes, Erlenmeyer flasks, beakers, measuring cylinders, volumetric pipettes, droppers, spatulas, glass funnels, ovens, spray bottles, universal pH paper, desiccators, porcelain crucibles, stirring rods, and pH meters.

The instrumental equipment included a Scanner electron microscopy (SEM, Sigma VP, UK) provides information regarding surface morphology, whereas XRD (Simens D500, UK) characterized the crystal structure of the sample. The carbon structures were assessed using Raman spectroscopy by $I_D/I_G$. BET isotherms (adsorption-desorption) and the pore size distribution method BJH were used to study the surface properties of the synthesized ternary composites in terms of surface area, pore diameter, and crystalline size. FT-IR shows the active groups present in GO and RGO. Transmission electron microscopy (CM 120, UK) gives a better picture of how the tube is put together. A Teflon-lined stainless-steel autoclave (China) was used during the synthesis process.

The chemical materials used were tin(II) chloride dihydrate ($SnCl_2{\cdot}2H_2O$, ≥98%), ferric chloride hexahydrate ($FeCl_3{\cdot}6H_2O$, ≥98%), graphite powder, potassium permanganate ($KMnO_4$), hydrogen peroxide ($H_2O_2$, 30%), sulfuric acid ($H_2SO_4$, 98%), hydrochloric acid (HCl, CDH India, 36%), phosphoric acid ($H_3PO_4$, Solvochem UK, 99.9%), hydrazine hydrate (Thomas, 80%), polyvinyl pyrrolidone (PVP, Direvo Industrial Biotechnology, Germany, 99.9%), ammonium acetate (CDH India, 99.9%), ammonia solution ($NH_4OH$, Chem Lab Belgium, 99%), ethanol (Sigma-Aldrich, 99.9%), calcium carbonate ($CaCO_3$), sodium chloride (NaCl), deionized water, and crystal violet dye ($C_{25}N_3H_{30}Cl$, Sigma-Aldrich).

### *Procedure*

#### *Synthesis of Graphene Oxide (GO)*

Graphene oxide is prepared by oxidizing pure powder graphite using a modified Hummers method. In this method, 0.225 g of graphite powder is added to a mixture containing strong oxidizing solutions, 27 mL of sulfuric acid ($H_2SO_4$) and 3 mL of phosphoric acid ($H_3PO_4$) (volume ratio of 9:1). 1.32g of potassium permanganate ($KMnO_4$) was added to the solution slowly. The mixture was stirred for 6 hours until a dark green solution was obtained. To remove the excess of permanganate ($KMnO_4$), 0.675mL of hydrogen peroxide ($H_2O_2$) was added to the solution in the form of slow drops while stirring for 10 minutes. The reaction is exothermic, so it is left overnight to cool down. Then the liquid is eliminated, and the solution is washed by mixing 10 mL of hydrochloric acid (HCl) with 30 mL of deionized water and continuing washing until the acidic function is

reached (pH = 7) and the precipitate was washed using a centrifuge at 5000 rpm for 7 minutes [21].

*Synthesis of Reduced Graphene Oxide (rGO)*

Graphene oxide is reduced using hydrazine hydrate by a hydrothermal method in an autoclave. 0.3 g of graphene oxide is mixed with 100 mL of deionized water and the solution is dispersed by a shaker for 3 hours. Then 0.12 mL of hydrazine hydrate was added. Then it was transferred into a Teflon-lined stainless-steel autoclave, which was heated to 80 °C for 12 hours. Furthermore, the precipitate is washed with water and ethanol, the RGO precipitate was dried in an oven at 60 °C [22].

*Synthesis of Iron Oxide Particles ($Fe_2O_3$)*

$Fe_2O_3$ nanoparticles are synthesized using the hydrothermal method. In brief, 0.405 g of $FeCl_3.6H_2O$, 0.116 g of ammonium acetate $NH_4AC$, and 0.750 g of polyvinyl pyrrolidine (PVP) were dissolved in 30 mL of deionized water. The mixture is stirred vigorously for 10 minutes until complete dissolution. Then it was transferred to a lined stainless-steel Teflon autoclave. At 140°C for 12 hours before cooling completely to laboratory temperature. The product of $Fe_2O_3$ is collected in a centrifuge, washed with distilled water and ethanol several times, and dried at 80 °C for 10 hours [23].

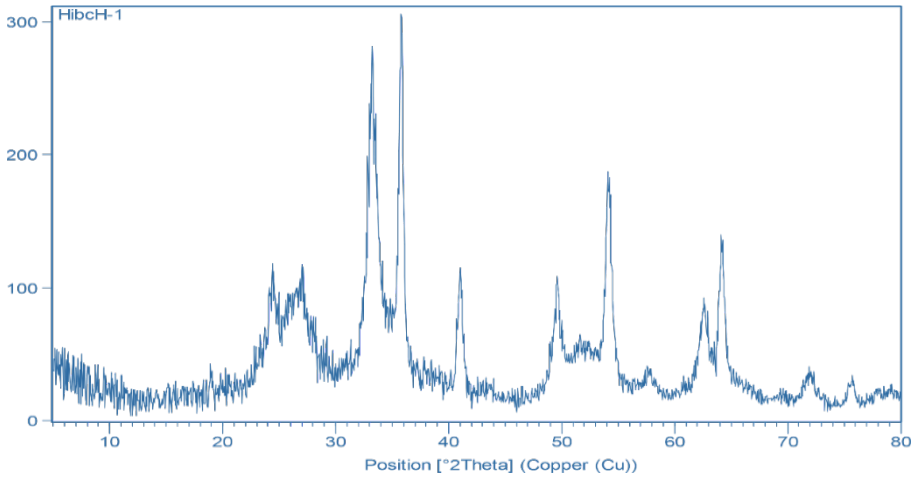


Fig. 1. X-ray diffraction pattern ternary composite ($SnO_2$-$Fe_2O_3$@RGO).

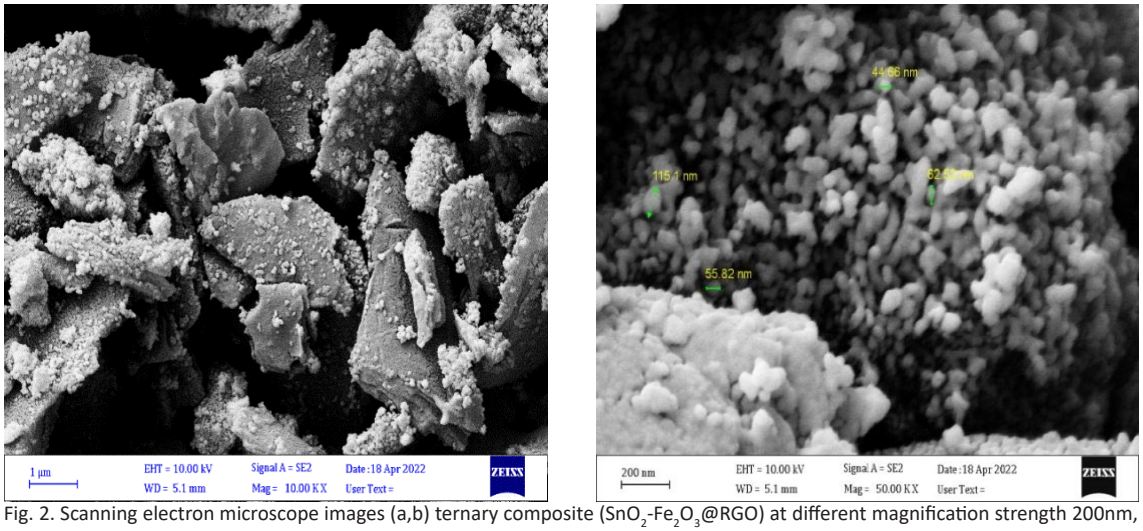


Fig. 2. Scanning electron microscope images (a,b) ternary composite ($SnO_2$-$Fe_2O_3$@RGO) at different magnification strength 200nm, 1µm.

*Synthesis of Tin Oxide ($SnO_2$) Nanoparticles*

By chemical precipitation, nano tin oxide ($SnO_2$) was prepared. In this method, dissolving. In 100 mL of deionized water, dissolve 2 g (0.1M) stannous chloride dehydrate ($SnCl_2.2H_2O$). ammonia solution was added with continuous stirring. It appears as a gel that is filtered and dried at 80 °C for 24 h [24].

*Synthesis of ($SnO_2/Fe_2O_3$@rGO) Composite*

Hydrothermal synthesis was used to create the ternary composite ($SnO_2/Fe_2O_3$@RGO). Following usual operating procedure, 0.2 g of reduced graphene oxide was shaken for one hour in 70 mL of a solution containing 30 mL of $H_2O$and 40 mL of $C_2H_5OH$.In addition, 0.3 g of tin oxide ($SnO_2$) and 0.5 g of iron oxide ($Fe_2O_3$) were added. The mixture was autoclaved at 170°C for 4h, then cooled to room temperature before the precipitate was collected and dried at 60°C [25]. It absorbs crystal violet dye.

**Characterization of the composite**

The synthesized $SnO_2/Fe_2O_3$@RGO composite was characterized to confirm its successful formation and to evaluate its suitability for dye

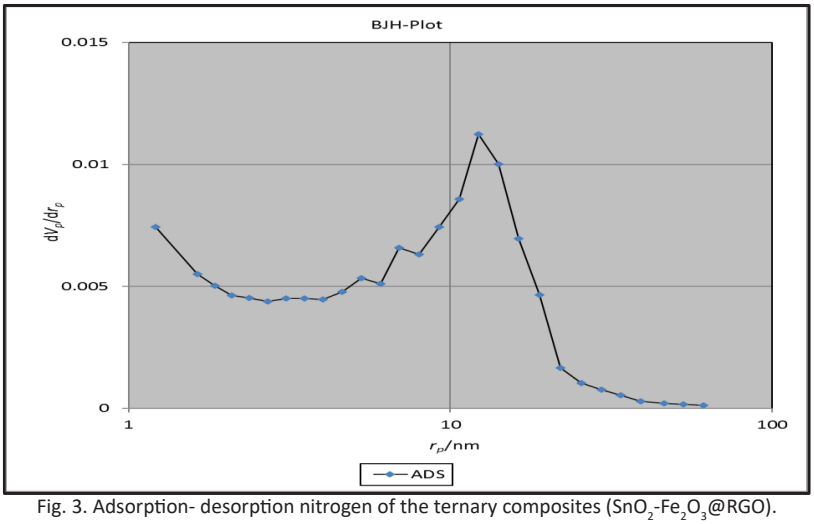


Fig. 3. Adsorption- desorption nitrogen of the ternary composites ($SnO_2$-$Fe_2O_3$@RGO).

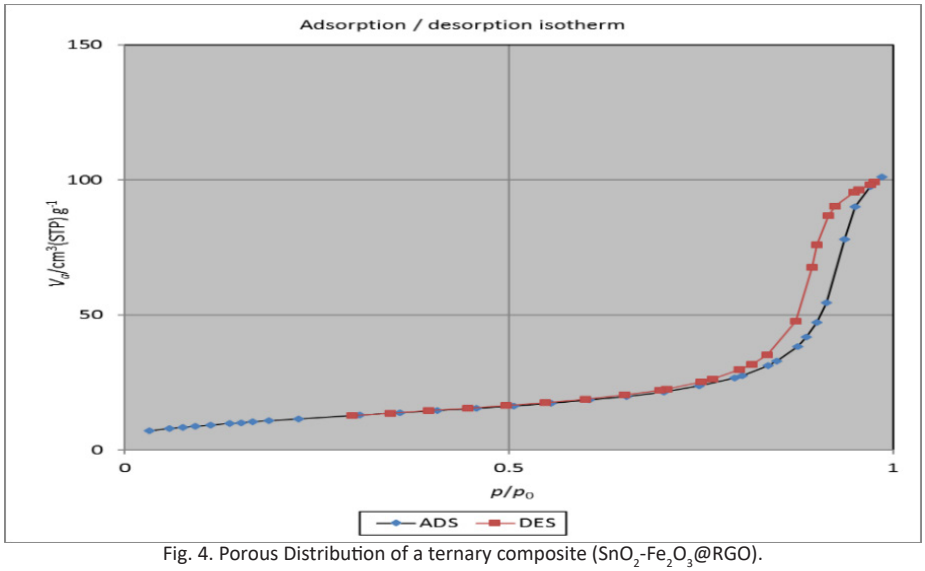


Fig. 4. Porous Distribution of a ternary composite ($SnO_2$-$Fe_2O_3$@RGO).

adsorption.

*X-ray diffraction (XRD) for $SnO_2/Fe_2O_3$@RGO*

RGO diffraction peaks cannot be seen in (Fig. 1) because the ordered structure of natural graphite flake was broken in the GO preparation process and GO reassembly was inhibited by $SnO_2$ and $Fe_2O_3$ growth on the RGO surface in the hydrothermal process. Diffraction peak relative intensities at 2 = 24.4°, 35.8°, 41.01°, 49.6°, 54.13°, 57.6°, 62.62°, and 64.17° $Fe_2O_3$. In the case of $SnO_2$, there are three distinct peaks in the $SnO_2$ crystal at temperatures of 26.73°, 33.21°, and 54.1°. According to these findings, $SnO_2$ and $Fe_2O_3$ do exist [26,27]. Only the pure phase was found. $SnO_2/Fe_2O_3$@RGO composites don't seem to have any RGO diffraction peaks, which may be because the RGO diffraction intensity of the composite is low [28].

*Filed emission Scanning Electron Microscopy for ($SnO_2$-$Fe_2O_3$@RGO)*

The Fig. 2 illustrated an abundance of nanoparticles affixed to sponge-like layers, to the degree that the layers had a coarse texture, indicating the homogeneous layering of metal oxides on graphene oxide layers. Image that may be caused by the aggregation and/or excess of metal oxides. The elemental analysis of $SnO_2$-$Fe_2O_3$@RGO nanocomposites by SEM-EDX revealed that the nanomaterial was made of Fe, Sn, O, and C with 3.2 % chloride contamination from the $FeCl_3.6H_2O$ due to poor washing of the nanocomposite yield [29].

*Surface area (BET, BJH)*

The BET isotherms (adsorption-desorption) and the BJH pore size distribution method was used to investigate the surface properties of the produced ternary composites in terms of surface area, pore diameter, and crystal size. Adsorption and adsorption isotherms for nitrogen are shown on the overlap in (Fig. 3). Surface pores are shown to be aggregated into plates that appear to be non-hardened [30]. By using the BJH method, the surface of the ternary composite was found to have an estimated pore diameter rate (16.15 nm) of 0.1564 $cm^3/g$. The porous diameter rate of the ternary composites showed that it has fine pores with sizes between 2 and 50 nm.as shown in (Fig. 4).

Other available instruments, such as FT-IR, UV–Vis, and TEM, were used for supporting analyses, but were not the focus of this study.

*Preparation of Crystal Violet Dye solution*

0.0125 grams of crystal violet dye were solubilized in 500 mL of distillated water to make the standard solution. Using the correct dilution, A series of solutions were used to prepare the reference solution. To change the pH, either 0.1 M NaOH or HCl were used. Fig. 5. illustrates the crystal violet solution and chemical composition.

*Batch Adsorption Experiments*

tests were conducted in a baker with a capacity of 250 mL that featured mechanical vibrators. In order to determine the influence that weight has on ternary composites, weights ranging from 0.01-0.06 g were deducted from the surface that had been adsorbed until equilibrium at 25°C was achieved. For the purpose of computing the time effect, various time intervals ranging from 1 to 140 minutes were used. and with a surface

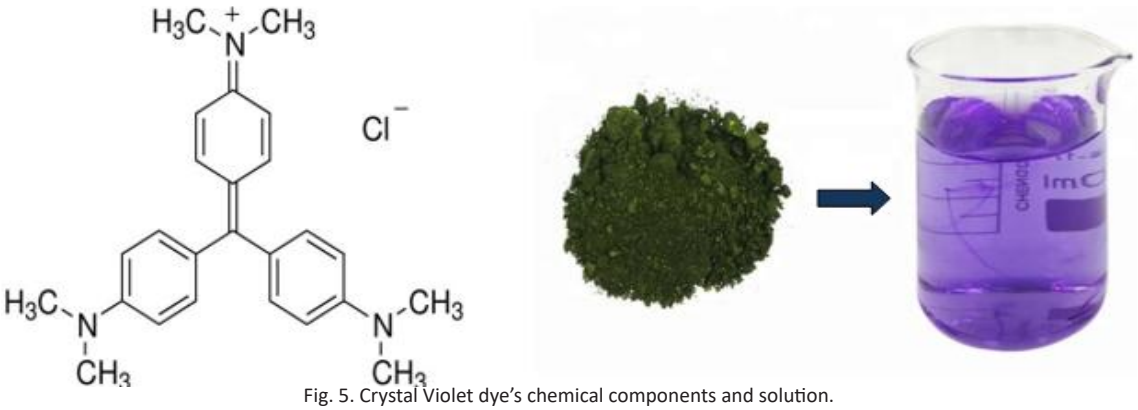


Fig. 5. Crystal Violet dye's chemical components and solution.

weight that had been calculated in advance. The pH scale was applied to ascertain how acidic functions impacted the system (4,6,8, and 10). The influence of temperature was investigated using a wide range of temperatures, ranging from 5 to 35 degrees Celsius. Utilizing a UV-Visible single-beam apparatus at 1200 nm, we were able to determine the absorbance at a wavelength of 585.5 nm. It is possible to calculate the amount of adsorbent by using the equation (1).

$$q_e = V(C_\circ - C_e)/m \quad (1)$$

$$R\% = 100\left(1 - \frac{C_e}{C_\circ}\right) \quad (2)$$

The volume of this solution has a volume of L, the CV dye concentrations C° and Ce are measured in mg. $L^{-1}$, the weight (m) of the ternary composites employed in the experiment is given in grams (g) and Removal percentage (R%).

## RESULTS AND DISCUSSION

A UV–Vis spectrophotometer was employed to determine the initial concentrations of crystal violet dye solutions prior to the adsorption experiments. The absorbance measurements were taken at a maximum wavelength ($\lambda_{max}$) of 580 nm. A calibration curve was constructed over a concentration range of 1–9 mg /L and was used to estimate the dye concentrations. Detailed information about the calibration curve is provided in the supplementary file (Fig. S1).

*Effect of adsorbent dosage*

According to studies, the removal efficiency of crystal violet dye increased from 40.9% to 94.9% when the amount of ternary composite powder adsorbent was increased from 0.01 to 0.06 g and a concentration of 25 mg /L at 25°C. This was due to an increase in the number of active sites on the adsorbent, but the adsorption capacity of the ternary composite powder adsorbent decreased from 20.5 to 51.2 mg/g. There is a higher clearance of crystal violet dye per unit weight of adsorbent because the dye is more easily accessible to the ternary composite surface at lower adsorbent concentrations. Due to very fast superficial adsorption onto the ternary composite surface at higher adsorbent masses, which results in a lower concentration of crystal violet dye in the solution than when the adsorbent dose is lower, some of the adsorption sites on the ternary composite adsorbent's surface remain empty during the

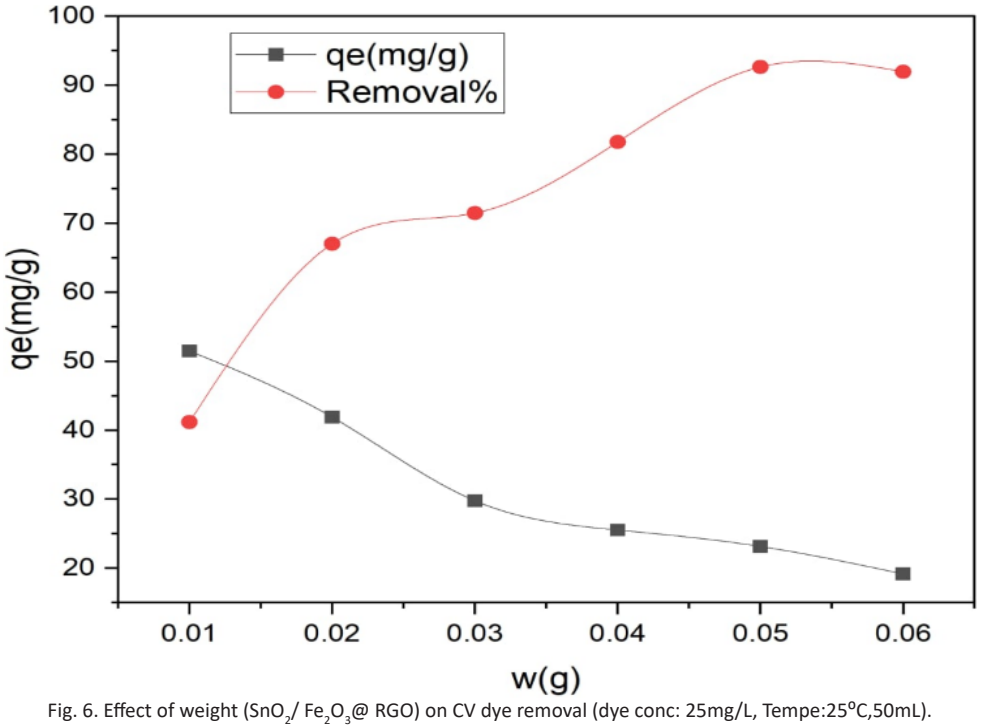


Fig. 6. Effect of weight ($SnO_2$/ $Fe_2O_3$@ RGO) on CV dye removal (dye conc: 25mg/L, Tempe:25°C,50mL).

adsorption process [31]. Therefore, as adsorbent amounts increase from 0.01 to 0.06g, the amount of crystal violet dye absorbed per unit mass of adsorbent decreases [32]. Additionally, a decrease in the total surface area and an increase in the length of the diffusion path brought on by the adsorbent's adsorption active sites aggregating or overlapping may be the cause of the decreased adsorption capacity. These outcomes concur with the research findings published in [33, 34]. Therefore, 0.01g was the ideal adsorbent dose for amount of adsorbent crystal violet dye from

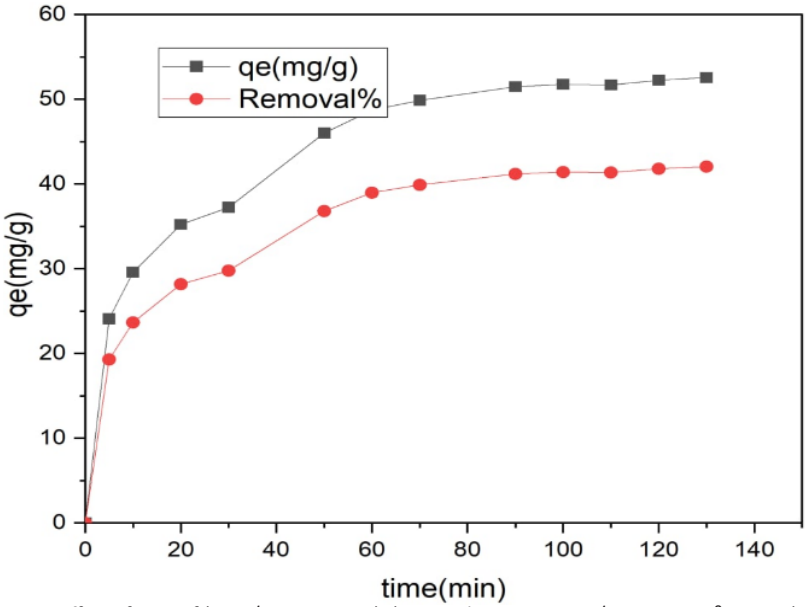


Fig. 7. Effect of time of ($SnO_2$/ $Fe_2O_3$@ RGO) :(0.01 g, dye conc:25 mg/ L, Tempe 25° C,50mL).

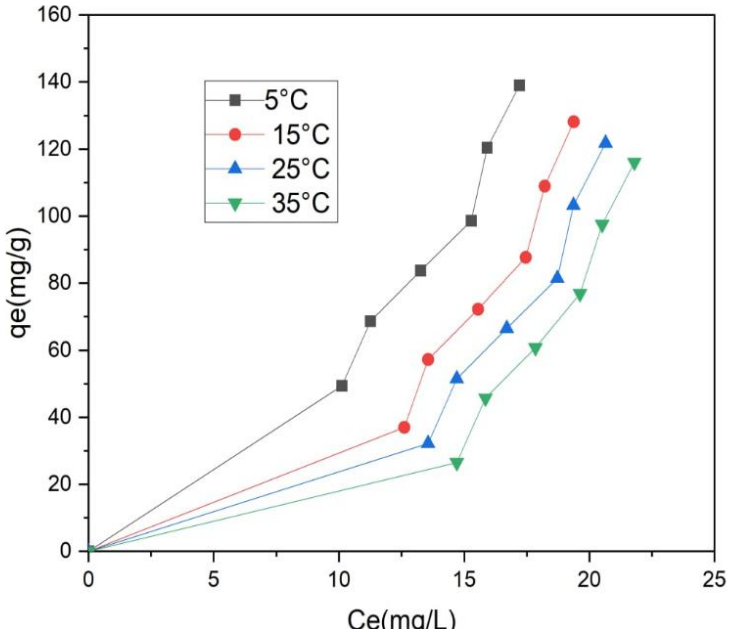


Fig. 8. Effect of temperature ($SnO_2$/ $Fe_2O_3$@ RGO):0.01 g (Dye conc:25 mg / L, Tempe 5- 35° C, 50mL).

ternary composite powder adsorbent. shown in Fig. 6.

*Effect of contact time*

The first few minutes of dye adsorption are extremely fast. Since the compound's surface area is so large, it can easily take up and absorb the dyes ($SnO_2$, $Fe_2O_3$, and RGO). The majority of the dye is eliminated as a result of the active groups present on the surface [35]. Color absorption increased with time throughout the first several minutes until equilibrium was reached [36] as illustrated in Fig. 7.

*Effect of Temperature*

The influence of temperature on the adsorption of crystal violet dye onto the $SnO_2/Fe_2O_3$@ RGO composite was investigated within the range of 5–35 °C [37]. As shown in Fig. 8, the adsorption capacity decreased with increasing temperature, indicating that the adsorption process is exothermic in nature. The decrease in adsorption performance at elevated temperatures can be attributed to the weakening of interactions between dye molecules and active sites on the adsorbent surface. This may result from increased molecular motion, which reduces the probability of dye molecules being retained on the adsorbent surface [38,39].

*Effect of pH*

The pH of the solution plays a critical role in the adsorption process, as it influences both the surface charge of the adsorbent and the ionization state of the dye molecules. Batch adsorption experiments were conducted at different pH values (4, 6, 8, and 10) under constant operating conditions. The results are illustrated in Fig. 9. At pH values lower than 4, the adsorbent surface becomes positively charged due to the presence of excess $H^+$ ions, which leads to electrostatic repulsion between the surface and the cationic crystal violet (CV) dye, resulting in reduced adsorption efficiency. As the pH increases, the concentration of $H^+$ ions decrease, and the surface of the adsorbent becomes more negatively charged. This enhances the electrostatic attraction between the CV dye molecules and the adsorbent surface, leading to an increase in dye removal efficiency. This behavior is consistent with previous findings [40–42], where the adsorption of CV dye was favored under alkaline conditions. The highest removal

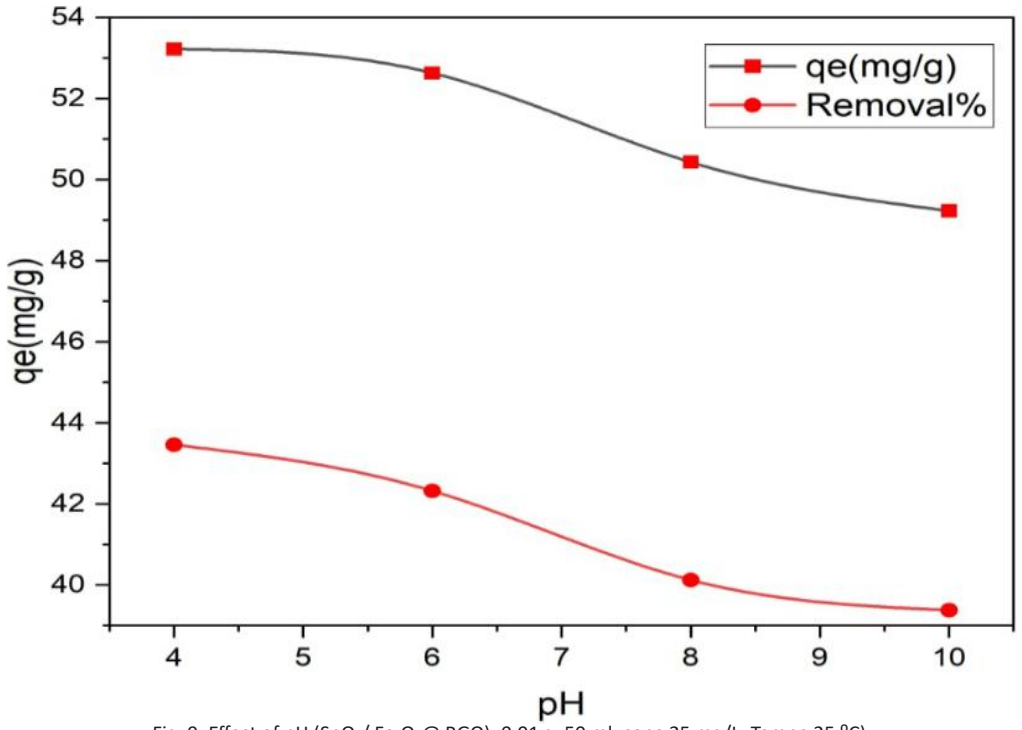


Fig. 9. Effect of pH ($SnO_2$/ $Fe_2O_3$@ RGO): 0.01 g, 50 ml, conc:25 mg/L. Tempe 25 °C).

efficiency was observed at pH 10, indicating that basic media provide favorable conditions for CV adsorption onto the ternary composite adsorbent.

*Effect of Ionic Strength*

The ionic strength of the solution significantly affects the adsorption process by influencing the interaction between the adsorbate and the adsorbent surface. In this study, the effect of different ionic strengths was examined using $CaCO_3$ and NaCl salts at concentrations ranging from 0.01 to 0.06 g, as shown in Fig. 10. An increase in salt concentration led to a noticeable decrease in the removal efficiency of crystal violet (CV) dye. This reduction can be attributed to the competition between the cationic dye molecules and the cations from the added salts for the available active sites on the surface of the adsorbent. As the ionic strength increases, more cations from the salts occupy these active sites, thereby reducing the accessibility of CV dye molecules to the surface. Furthermore, the electrostatic shielding effect becomes more pronounced at higher ionic strengths, which weakens the electrostatic attraction between the negatively charged adsorbent surface and the positively charged dye molecules. This behavior aligns with previous studies [43–45], which reported that elevated ionic strength can suppress dye adsorption due to increased ion competition and reduced electrostatic interactions.

*Adsorption isotherm*

The heterogeneous energy of the active site causes the S-type adsorption isotherm to stay in line with Freundlich and Temkin for multi-layer adsorption. As seen in Fig. 11 and Table 1, this type illustrates that strong adsorption takes place on the solvent because of an attractive interaction that exists between the molecules of the adsorbent material and the adsorbent surface [46]. It demonstrates that adsorption studies and Freundlich isotherms are compatible. According to the Langmuir isotherm, monolayer adsorption occurs on a homogenous, uniform surface with a finite number of adsorption sites. The following is a mathematical representation of this equation:

$$C_e/q_e = 1/Kl + (a/K_l).C_e \quad (3)$$

The Freundlich isotherm, in contrast, describes the process of reversible and non-

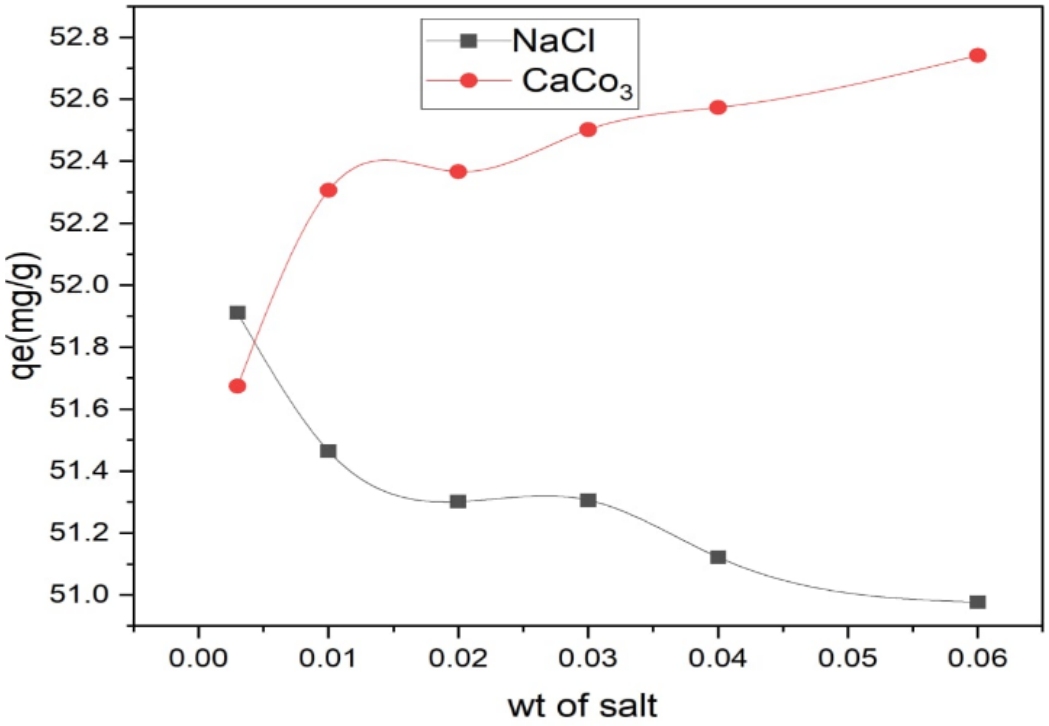


Fig. 10. Effect of ionic strength (Dye conc:25 mg/L, Tempe 25° C, ($SnO_2$/ $Fe_2O_3$@ RGO):0.01 g).

ideal adsorption on heterogeneous surfaces. It accounts for interactions between adsorbed molecules and indicates that the sorption energy decreases exponentially as the adsorption sites on the adsorbent are progressively occupied. The Freundlich isotherm is calculated using the equation:

$$\log q_e = \log K_F + \frac{1}{n}\log C_e \quad (4)$$

Meanwhile, the Temkin model highlights that the interaction between the adsorbate and the adsorbent leads to a gradual decline in the heat of sorption as coverage increases. This relationship is described by the equation:

$$q_e = B \ln A_t + B \ln C_e \quad (5)$$

In this case, Ce represents the equilibrium concentration (mg/L) and indicates the amount of Crystal Violet dye adsorbed at equilibrium (mg/g). KL is the Langmuir constant, while the value qm is the estimated maximal adsorption capacity. Furthermore, the Temkin adsorption potential is indicated by At, and the Freundlich constants are KF and 1/n.

*Adsorption kinetic*

Pseudo first order and pseudo second order

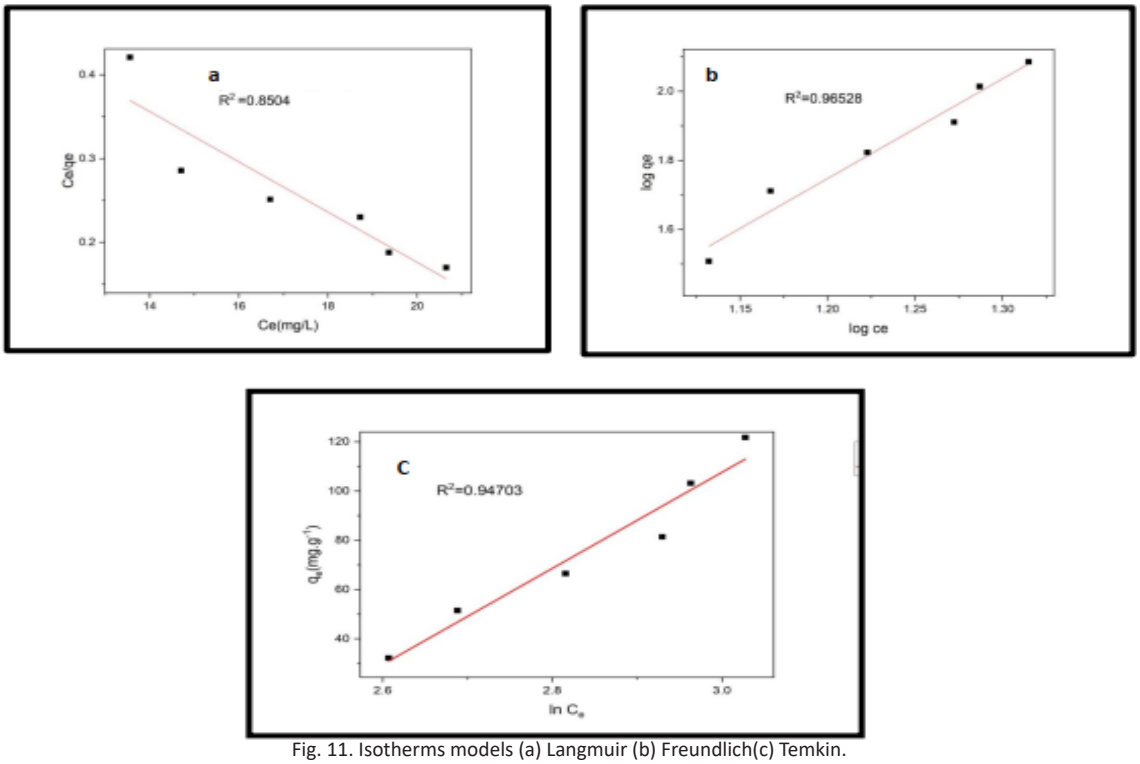


Fig. 11. Isotherms models (a) Langmuir (b) Freundlich(c) Temkin.

Table 1. Langmuir, Freundlich, and Timken equations were used to calculate the crystal violet uptake of ternary composites at 25°C.

| | | | |
|---|---|---|---|
| Langmuir | $R^2$ | $Q_{max}$(mg/g) | $K_L$(L/mg) |
| | 0.85040 | -78.7401 | -0.1027 |
| Freundlich | $R^2$ | N | Kf(mg/g) |
| | 0.96528 | 2.6853 | 3.6738 |
| Temkin | $R^2$ | B | At |
| | 0.94703 | 24.9983 | 0.7012 |

equation models were used to investigate the rate of (CV) dye adsorption on ternary composites ($SnO_2/Fe_2O_3$@RGO). Tables of kinetic, qe, and $R^2$ values can be found at the bottom of this Table 2. Using the pseudo second order model and the amount ($R^2$ = 0.9969), if the correlation coefficient $R^2$ is determined to be strong, the dye's adsorption kinetics will fit the pseudo second order model [47,48].

$$\text{pesudo} - \text{first order}: \ln(\text{qe} - \text{qt}) = \ln \text{qe} - \text{k}_1\text{t} \quad (6)$$

qt is the quantity adsorbed at time t, qe is the amount adsorbed at equilibrium (in mg. $g^{-1}$), and t is the period (min). By displaying ln(qe-qt) as a function of time t, one can derive the rate constant k1 for the adsorption process ($min^{-1}$).

$$\text{pesudo} - \text{second order}: \frac{\text{t}}{\text{qt}} = \frac{1}{\text{K}_2\text{qe}^2} + \frac{1}{\text{q}_\text{e}} \quad (7)$$

the pseudo-second order constant $K_2$ (1/mg.1/min) and equilibrium adsorbate concentration per gram of adsorbent (mg/g) qe can be derived empirically from the slope and y-axis of the t/qt line as a function of time.

*Thermodynamic variables.*

Analysis of crystal violet adsorption on ($SnO_2/Fe_2O_3$@RGO) was done using the following thermodynamic factors: Changes in the Gibbs free energy (ΔG°), enthalpy (ΔH°), and entropy. They were calculated using the following formulas.

$$\text{K}_\text{d} = \frac{\text{q}_\text{e}}{\text{C}_\text{e}} \quad (8)$$

$$\Delta G° = \text{-RTlnK}_\text{d} \quad (9)$$

$$\ln\text{K}_\text{d} = \frac{\Delta\text{S}°}{\text{R}} - \frac{\Delta\text{H}°}{\text{R}} \cdot \frac{1}{\text{T}} \quad (10)$$

Ce is the equilibrium concentration for an ideal gas (R = 8.314 J/mol.K), Ce is the starting concentration (mg/L), T is the absolute temperature (K), Kc is the coefficient of distribution, and R is the ideal gas constant (mg./L).

The linear graph of lnKd vs 1/T in Fig. 12 shows how temperature affects the ternary composite's ability to remove Crystal Violet dye throughout the adsorption process. Furthermore, Table 3 presents the correlation coefficients and estimated thermodynamic parameters. Gibbs free energy (ΔG°) = -1.7570 $kJ.mol^{-1}$ under constant reaction conditions, whereas entropy (ΔS°) and enthalpy (ΔH°) were found to be -42.4820 J/mol.K and -14.6592 KJ/mol, respectively. This suggests that within the temperature range under investigation, the adsorption of Crystal Violet dye onto the adsorbent surface occurred spontaneously. The data analysis clearly shows that spontaneous single-layer adsorption, which is a sign of chemical adsorption, and multi-layer adsorption, which is a sign of physical adsorption, took place during the procedure. This suggests that both physical and chemical interactions were involved in the adsorption of Crystal Violet dye onto the $SnO_2$-$Fe_2O_3$@RGO surface. ΔG° normally ranges between 0 and 20 kJ/mol for physical adsorption, whereas for combined chemical-physical adsorption, it falls between 20 and 80 $kJ.mol^{-1}$. Chemical adsorption alone is reported to exhibit values spanning 80 to 400 kJ/mol for reaction enthalpy changes. According to some studies, ΔH° values for physical adsorption range up to 21 kJ/mol, for chemical-physical adsorption they vary between 21 and 80 kJ/mol, and for purely chemical adsorption they are reported between 80 and 200 kJ/mol. Negative ΔH° values and the observed decrease in Kd with rising temperature suggest that the adsorption of Crystal Violet dye on the ternary composite surface was exothermic[45,46,49]. The reduction in ΔG° values with increasing temperature further confirms that higher temperatures are unfavorable for the adsorption process. As the temperature rises, desorption occurs more readily, weakening the adsorption capacity. This reduction can be attributed to increased molecular motion at elevated temperatures, which disrupts the bonds and results in the release of Crystal Violet dye from the $SnO_2$-$Fe_2O_3$@RGO surface. The relatively low ΔS° values indicate no significant change in

Table 2. Kinetics parameters for the adsorption of CV by ternary adsorbent composites.

| Dye | Pseudo -First Order | | | Pseud-Second Order | | |
|---|---|---|---|---|---|---|
| | $k_1$ (1/min) | Qe (mg/g) | $R^2$ | $K_2$ (1/mg.1/min) | $q_e$ (mg/g) | $R^2$ |
| Crystal violet | -0.00034 | 37.3484 | 0.97859 | 0.00206 | 55.30973 | 0.9969 |

system entropy during the adsorption process. The negative ΔS° values suggest lower disorder at the interface of the liquid and solid phases during Crystal Violet dye adsorption. Conversely, an increase in disorder might occur when dye molecules are released from the solid adsorbent into the solution phase [50, 51].

*Recovery and regeneration of spent adsorbents Cycling*

The efficiency of regeneration was measured during five successive cycles, each beginning with an adsorption equilibration phase and ending with desorption. The adsorption studies were carried out with the following parameters: an adsorbent dose of 0.01 g, pH of 7, duration of 90 minutes, and temperature of 298 K. Following the adsorption procedure, the granules were washed with distilled water. After desorption, samples were collected using a pipette and spun at 180 rpm for 2 minutes using a Beckman Coulter J326XPI-IM-1 centrifuge. The final concentration was determined using a spectrophotometer. Cycling stability is an important feature to consider when assessing the potential of an adsorbent material. To evaluate the material's regenerative capacity, five-cycle adsorption-desorption tests were performed. Fig. 13 shows that as the number of cycles rose, the adsorption capacity gradually decreased. However, after five cycles, the adsorption capacity may have fallen to 55.4% of its original value. The ternary composite outperformed other materials in terms of adsorption stability, retaining its performance without considerable degradation. These results show the $SnO_2$-$Fe_2O_3$@RGO composite's great reusability and regeneration capabilities.

*Comparison of crystal violet dye with other sorbents*

The comparison of various adsorbents' monolayer adsorption capabilities with the current work is shown in Table 4. The table indicates that the adsorbent has a higher adsorption capacity for crystal violet dye compared to other adsorbents. The $SnO_2$-$Fe_2O_3$ @RGO material has the potential to remove harmful crystal violet dye from aqueous

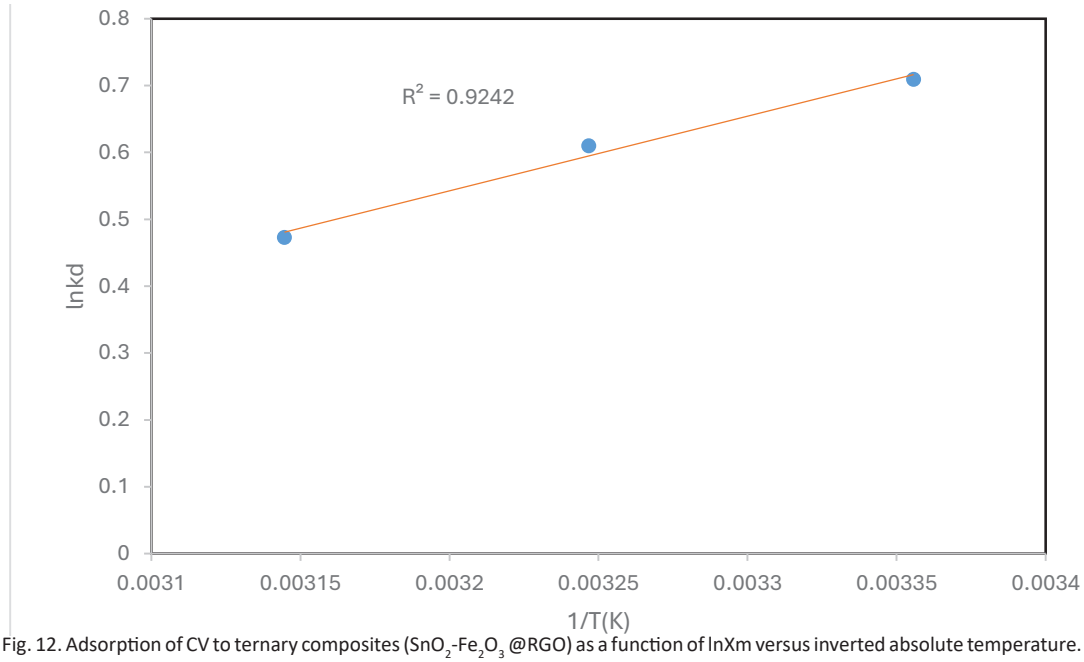


Fig. 12. Adsorption of CV to ternary composites ($SnO_2$-$Fe_2O_3$ @RGO) as a function of lnXm versus inverted absolute temperature.

Table 3. Shows the thermodynamic functions of CV adsorption on ternary composites ($SnO_2$-$Fe_2O_3$ @RGO) at 25°C.

| Adsorbate | ΔG (kJ/mol) | ΔH (kJ/mol) | ΔS (J/k.mol) |
|---|---|---|---|
| $SnO_2$-$Fe_2O_3$ @RGO | -1.7570 | -14.6592 | -42.4820 |

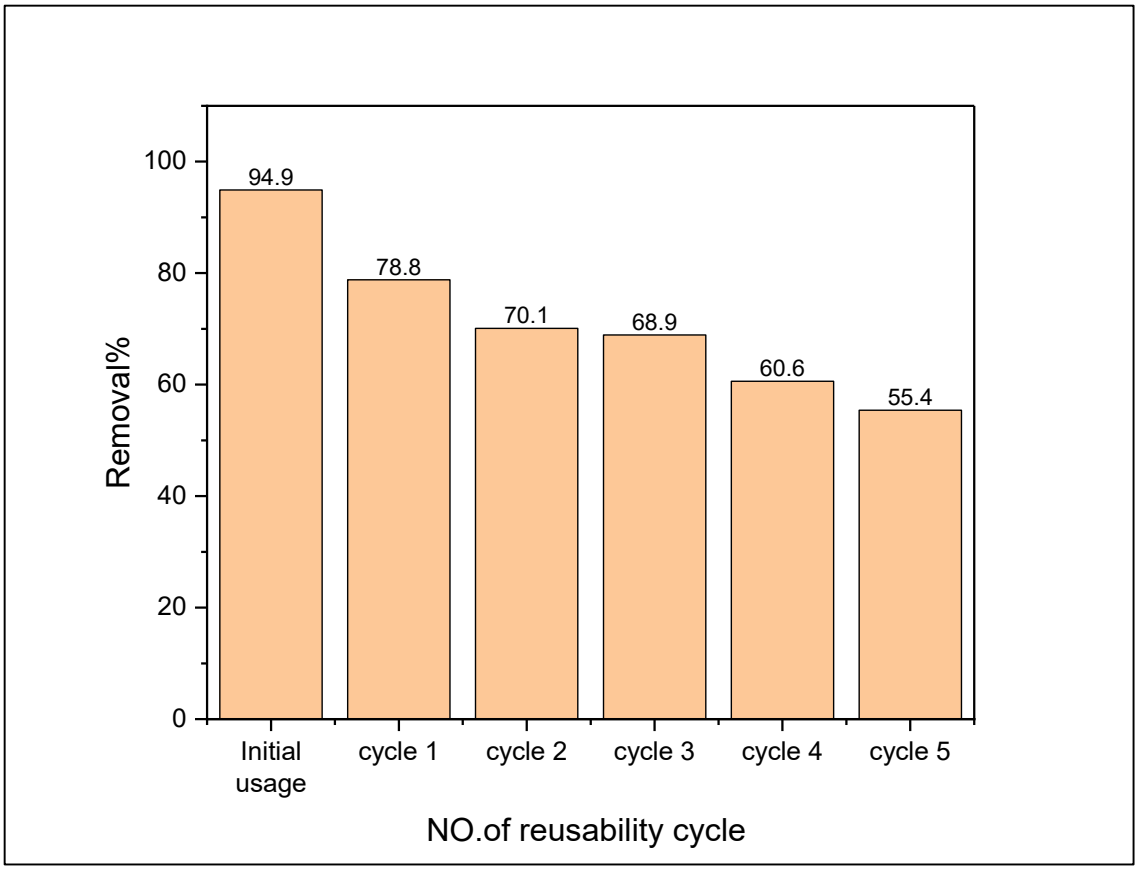


Fig. 13. Reusability of $SnO_2$-$Fe_2O_3$ @RGO for the removal of C.V dye from water for five runs.

Table 4. Comparison of adsorption capacities of different adsorbents for crystal violet dye.

| Adsorbent | $q_{max}$(mg. $g^{-1}$) | Reference |
|---|---|---|
| MWCNTs/$Mn_{0.8}Zn_{0.2}Fe_2O_4$ nanoparticle | 5 | [52] |
| Raw cassava peels powder | -5.15 | [53] |
| Poly(benzofuran-co-arylacetic acid)-FA | 25.10 | [54] |
| Activated Carbon/$Fe_3O_4$ | 35.31 | [55] |
| P(AAm-MA)/MMT | 20.36 | [56] |
| PVA/PAA-hBN@PDA fiber | 793.65 | [57] |
| $ZrO_2$ @$MnCO_3$ @$CdCO_3$ nanocomposite | 179.52 | [58] |
| Chitin-psyllium based aerogel | 227.11 | [54] |
| $SnO_2/Fe_2O_3$@RGO | 51.2 | Present study |

solutions and industrial waste.

## CONCLUSION

The equilibrium time for CV adsorption on the composite's surface is ninety minutes. As the solution's acidity function declines, the concentration of CV dye adsorbent on the adsorbent's surface increases. It was discovered that the Freundlich isotherm model and the adsorption isotherms were compatible. The pseudo-second-order equation can be used to the kinetics of adsorption to explain the binding of dye to the adsorbent surface. With measured enthalpy (ΔH) values below 40 kj/mol, the physical nature of the dyes' adsorption on the composite surface is demonstrated. Given the existence of negative

free energy change (ΔG) values, the adsorption of CV dye is a spontaneous process.

## ACKNOWLEDGMENT

Researchers thank the University Al-Qadisiyah, College of Science, for their assistance.

## CONFLICT OF INTEREST

The authors declare that there is no conflict of interests regarding the publication of this manuscript.

## REFERENCES

1. A study on graphene oxide and its nanocomposites: preparation, properties and applications in water and wastewater treatment. Comprehensive Analytical Chemistry: Elsevier; 2024. p. 705-720.
2. Mushahary N, Sarkar A, Basumatary F, Brahma S, Das B, Basumatary S. Recent developments on graphene oxide and its composite materials: From fundamentals to applications in biodiesel synthesis, adsorption, photocatalysis, supercapacitors, sensors and antimicrobial activity. Results in Surfaces and Interfaces. 2024;15:100225.
3. Yang J, Shojaei S, Shojaei S. Removal of drug and dye from aqueous solutions by graphene oxide: Adsorption studies and chemometrics methods. npj Clean Water. 2022;5(1).
4. Vassileva P, Tumbalev V, Kichukova D, Voykova D, Kovacheva D, Spassova I. Study on the Dye Removal from Aqueous Solutions by Graphene-Based Adsorbents. Materials. 2023;16(17):5754.
5. Al-Kadhi NS, Al-Senani GM, Saad FA, Munshi AM, Abdelrahman EA. Modification of nickel ferrite nanoparticles by sodium docusate surfactant for superior crystal violet dye removal from aqueous solutions. Scientific Reports. 2024;14(1).
6. Murshid N, Mouhtady O, Abu-samha M, Obeid E, Kharboutly Y, Chaouk H, et al. Metal Oxide Hydrogel Composites for Remediation of Dye-Contaminated Wastewater: Principal Component Analysis. Gels. 2022;8(11):702.
7. Lavrynenko O, Zahornyi M, Pavlenko O. Some aspects of adsorption, catalytic and photocatalytic interactions of organic dyes with $TiO_2$-based binary nanocomposites. Nano Studies. 2024.
8. Erden L, Deveci İ, Erden H. Nonlinear Kinetics and Isotherm Modeling of Rhodamine B Adsorption onto $Al_2O_3$ Decorated Laponite. ACS Omega. 2026;11(12):18805-18813.
9. Singh KP, Wareppam B, Raghavendra KG, Singh NJ, de Oliveira AC, Garg VK, et al. Heterophase Grain Boundary-Rich Superparamagnetic Iron Oxides/Carbon Composite for Cationic Crystal Violet and Anionic Congo Red Dye Removal. Adv Eng Mater. 2023;25(22).
10. Wareppam B, Singh NJ, Singh KP, Aomoa N, Singh LH. Imidazole-functionalized plasma-treated ZnO and α-$Fe_2O_3$ composites for catalytic degradation of dye. Int J Mod Phys B. 2023;38(24).
11. Tourani S. Preparation of multi-walled carbon nanotubes (MWCNT) and graphene oxide (GO) incorporated Cr-TA@SSZ composite metal-organic frameworks and their use as adsorbents for adsorptive removal of TPA, BA, and p-tol from wastewaters. Research Square Platform LLC; 2022.
12. Alsulami A. Batch Adsorption Kinetics and Isotherm Modeling of Thiocyanate Using GO-Metal Oxide Nanocomposites. Elsevier BV; 2026.
13. Konicki W, Hełminiak A, Arabczyk W, Mijowska E. Adsorption of cationic dyes onto Fe@graphite core–shell magnetic nanocomposite: Equilibrium, kinetics and thermodynamics. Chem Eng Res Des. 2018;129:259-270.
14. Ali G, Jazib Abbas Zaidi S, Abdul Basit M, Park TJ. Synergetic performance of systematically designed g-$C_3N_4$/rGO/$SnO_2$ nanocomposite for photodegradation of Rhodamine-B dye. Appl Surf Sci. 2021;570:151140.
15. Hynes NRJ, Kumar JS, Kamyab H, Sujana JAJ, Al-Khashman OA, Kuslu Y, et al. Modern enabling techniques and adsorbents based dye removal with sustainability concerns in textile industrial sector -A comprehensive review. Journal of Cleaner Production. 2020;272:122636.
16. Alkali Metal Cations Influence the $CO_2$ Adsorption Capacity of Nanosized Chabazite: Modeling vs Experiment. American Chemical Society (ACS).
17. Mittal H, Al-Alili A, Alhassan S. Adsorption Isotherm and Kinetics of Water Vapor Adsorption Using Novel Super-Porous Hydrogel Composites. ASME International; 2021.
18. Li Y, Yue Q, Gao B, Li Q, Li C. Adsorption thermodynamic and kinetic studies of dissolved chromium onto humic acids. Colloids Surf B Biointerfaces. 2008;65(1):25-29.
19. Rahman DA, Helmy Q, Syafila M, Gumilar A. Adsorption of Dyes Using Graphene Oxide-Based Nano-Adsorbent: A Review. Jurnal Presipitasi : Media Komunikasi dan Pengembangan Teknik Lingkungan. 2022;19(2):384-397.
20. Melchor-Durán AP, Moreno-Virgen MR, Bonilla-Petriciolet A, Reynel-Ávila HE, Lucio Ortiz E, González-Vázquez OF. Heavy Metal Removal from Water Using Graphene Oxide in Magnetic-Assisted Adsorption Systems: Characterization, Adsorption Properties, and Modelling. Separations. 2024;11(10):294.
21. Pang WK, Foo KL, Hashim U, Tan SJ, Voon CH, Ruslinda AR, et al. Physical and structural study of graphene oxide by improved hummers method. AIP Conference Proceedings: Author(s); 2018. p. 020035.
22. Alam SN, Sharma N, Kumar L. Synthesis of Graphene Oxide (GO) by Modified Hummers Method and Its Thermal Reduction to Obtain Reduced Graphene Oxide (rGO)*. Graphene. 2017;06(01):1-18.
23. Lin F, Wang H. $Fe_2O_3$–$SnO_2$–graphene films as flexible and binder-free anode materials for lithium-ion batteries. J Mater Res. 2015;30(18):2736-2746.
24. Kirthika V. Preparation and Characterization of Al doped $SnO_2$ Nanocrystalline Thin Films by Spray Pyrolysis Technique. International Journal for Research in Applied Science and Engineering Technology. 2020;8(2):183-191.
25. Zhu J, Lu Z, Oo MO, Hng HH, Ma J, Zhang H, et al. Synergetic approach to achieve enhanced lithium ion storage performance in ternary phased SnO2–$Fe_2O_3$/rGO composite nanostructures. J Mater Chem. 2011;21(34):12770.
26. Sheng W, Ma S, Li W, Liu Z, Guo X, Jia X. A facile route to fabricate a biodegradable hydrogel for controlled pesticide release. RSC Advances. 2015;5(18):13867-13870.
27. Da Silva LF, Lopes OF, Catto AC, Avansi W, Bernardi MIB, Li MS, et al. Hierarchical growth of ZnO nanorods over $SnO_2$ seed layer: insights into electronic properties from photocatalytic activity. RSC Advances. 2016;6(3):2112-2118.
28. Zhang H, Xie A, Wang C, Wang H, Shen Y, Tian X. Novel rGO/α-$Fe_2O_3$ composite hydrogel: synthesis, characterization and high performance of electromagnetic wave absorption. Journal of Materials Chemistry A. 2013;1(30):8547.
29. Suber P. OA dissertations at ProQuest. Front Matter; 2007. http://dx.doi.org/10.63485/dnexm-wcx08
30. Stankovich S, Dikin DA, Piner RD, Kohlhaas KA, Kleinhammes A, Jia Y, et al. Synthesis of graphene-based nanosheets via chemical reduction of exfoliated graphite oxide. Carbon.

2007;45(7):1558-1565.
31. Dyg Khairunnisa Awg Z, Norzita N, Muhd Asyiq A, Khairudin A. Utilization of Polyethylenimine (PEI) Modified Carbon Black Adsorbent Derived from Tire Waste for the Removal of Aspirin. J Pharm Pharmacol. 2019;7(4).
32. Sahu O, Singh N. Significance of bioadsorption process on textile industry wastewater. The Impact and Prospects of Green Chemistry for Textile Technology: Elsevier; 2019. p. 367-416.
33. Sabna V, Thampi SG, Chandrakaran S. Adsorption of crystal violet onto functionalised multi-walled carbon nanotubes: Equilibrium and kinetic studies. Ecotoxicol Environ Saf. 2016;134:390-397.
34. Tanhaei B, Ayati A, Iakovleva E, Sillanpää M. Efficient carbon interlayed magnetic chitosan adsorbent for anionic dye removal: Synthesis, characterization and adsorption study. Int J Biol Macromol. 2020;164:3621-3631.
35. Karam FF, Hassan FF, Hessoon HM. Adsorption of toxic crystal violet dye using (Chitosan- OMWCNTs) from aqueous solution. Journal of Physics: Conference Series. 2021;1999(1):012015.
36. Oguntimein GB. Biosorption of dye from textile wastewater effluent onto alkali treated dried sunflower seed hull and design of a batch adsorber. Journal of Environmental Chemical Engineering. 2015;3(4):2647-2661.
37. Alzayd AAM, Karam FF. Adsorption of Atenolol drug from Aqueous solution by poly (AAM_MA) hydrogel and used in Drug Delivery System: Study kinetic and Thermodynamic. Research Journal of Pharmacy and Technology. 2019;12(10):4678.
38. Tomul F, Arslan Y, Kabak B, Trak D, Kendüzler E, Lima EC, et al. Peanut shells-derived biochars prepared from different carbonization processes: Comparison of characterization and mechanism of naproxen adsorption in water. Sci Total Environ. 2020;726:137828.
39. Haleem A, Shafiq A, Chen S-Q, Nazar M. A Comprehensive Review on Adsorption, Photocatalytic and Chemical Degradation of Dyes and Nitro-Compounds over Different Kinds of Porous and Composite Materials. Molecules. 2023;28(3):1081.
40. Nawi MA, Sabar S, Jawad AH, Sheilatina, Ngah WSW. Adsorption of Reactive Red 4 by immobilized chitosan on glass plates: Towards the design of immobilized $TiO_2$–chitosan synergistic photocatalyst-adsorption bilayer system. Biochem Eng J. 2010;49(3):317-325.
41. Wanyonyi WC, Onyari JM, Shiundu PM. Adsorption of Congo Red Dye from Aqueous Solutions Using Roots of Eichhornia Crassipes: Kinetic and Equilibrium Studies. Energy Procedia. 2014;50:862-869.
42. Kim T, An B. Effect of Hydrogen Ion Presence in Adsorbent and Solution to Enhance Phosphate Adsorption. Applied Sciences. 2021;11(6):2777.
43. Khasri A, Ahmad MA. Adsorption of basic and reactive dyes from aqueous solution onto Intsia bijuga sawdust-based activated carbon: batch and column study. Environmental Science and Pollution Research. 2018;25(31):31508-31519.
44. Mouni L, Belkhiri L, Bollinger J-C, Bouzaza A, Assadi A, Tirri A, et al. Removal of Methylene Blue from aqueous solutions by adsorption on Kaolin: Kinetic and equilibrium studies. Applied Clay Science. 2018;153:38-45.
45. Al-Asadi ST, Al-Qaim FF. Adsorption of Methylene Blue Dye from aqueous solution using low cost adsorbent: Kinetic, Isotherm Adsorption and Thermodynamic Studies. Research Square Platform LLC; 2023.
46. Jabbar Almukhtar JG, Karam FF. Kinetic and Thermodynamic Studies for Mebeverine hydrochloride Adsorption from Aqueous Solution using prepared chitosan polymer in delivery drug system. Journal of Physics: Conference Series. 2020;1664(1):012062.
47. Safa F, Alinezhad Y. Ternary nanocomposite of $SiO_2/Fe_3O_4$/Multi-Walled Carbon Nanotubes for Efficient Adsorption of Malachite Green: Response Surface Modeling, Equilibrium Isotherms and Kinetics. Silicon. 2019;12(7):1619-1637.
48. Ghaedi M, Nasab AG, Khodadoust S, Rajabi M, Azizian S. Application of activated carbon as adsorbents for efficient removal of methylene blue: Kinetics and equilibrium study. Journal of Industrial and Engineering Chemistry. 2014;20(4):2317-2324.
49. Mohammadnia E, Hadavifar M, Veisi H. Kinetics and thermodynamics of mercury adsorption onto thiolated graphene oxide nanoparticles. Polyhedron. 2019;173:114139.
50. Vuković GD, Marinković AD, Čolić M, Ristić MĐ, Aleksić R, Perić-Grujić AA, et al. Removal of cadmium from aqueous solutions by oxidized and ethylenediamine-functionalized multi-walled carbon nanotubes. Chem Eng J. 2010;157(1):238-248.
51. Liu Y, Liu Y-J. Biosorption isotherms, kinetics and thermodynamics. Sep Purif Technol. 2008;61(3):229-242.
52. Gabal MA, Al-Harthy EA, Al Angari YM, Abdel Salam M. MWCNTs decorated with $Mn_{0.8}Zn_{0.2}Fe_2O_4$ nanoparticles for removal of crystal-violet dye from aqueous solutions. Chem Eng J. 2014;255:156-164.
53. Okorocha NJ, Omaliko CE, Osuagwu CC, Chijioke-Okere MO, Enenebeaku CK. Utilization of Agro-Waste in the Elimination of Dyes from Aqueous Solution: Equilibrium, Kinetic and Thermodynamic Studies. International Letters of Chemistry, Physics and Astronomy. 2021;86:11-23.
54. Ganea I-V, Nan A, Baciu C, Turcu R. Effective Removal of Crystal Violet Dye Using Neoteric Magnetic Nanostructures Based on Functionalized Poly(Benzofuran-co-Arylacetic Acid): Investigation of the Adsorption Behaviour and Reusability. Nanomaterials. 2021;11(3):679.
55. Foroutan R, Peighambardoust SJ, Peighambardoust SH, Pateiro M, Lorenzo JM. Adsorption of Crystal Violet Dye Using Activated Carbon of Lemon Wood and Activated Carbon/Fe3O4 Magnetic Nanocomposite from Aqueous Solutions: A Kinetic, Equilibrium and Thermodynamic Study. Molecules. 2021;26(8):2241.
56. Aref L, Navarchian AH, Dadkhah D. Adsorption of Crystal Violet Dye from Aqueous Solution by Poly(Acrylamide-co-Maleic Acid)/Montmorillonite Nanocomposite. J Polym Environ. 2016;25(3):628-639.
57. Azizi N, Eslami R, Goudarzi S, Zarrin H. Harnessing synergy: Polydopamine-hBN integration in electrospun nanofibers for Co (II) ion, methylene blue and crystal violet dyes adsorption. Chemosphere. 2024;363:142842.
58. Al-Kadhi NS, Abdelrahman EA, Alamro FS, Saad FA, Al-Raimi DS. Innovative nanocomposite comprising of ZrO2, MnCO3, and $CdCO_3$ for superior crystal violet dye adsorption: synthesis, characterization, and regeneration insights. Scientific Reports. 2025;15(1).